Available online at www.sciencedirect.com
SCIENCE DIRECT®
Journal of Sound and Vibration 283 (2005) 1093–1113
JOURNAL OF SOUND AND VIBRATION
www.elsevier.com/locate/jsvi

Three-dimensional natural vibration analysis and energy considerations for a piezoelectric rectangular plate

Piotr Cupiał*

Institute of Applied Mechanics, Cracow University of Technology, Al. Jana Pawła II-go 37, 31-864 Kraków, Poland

Received 23 September 2003; received in revised form 9 March 2004; accepted 3 June 2004
Available online 11 November 2004

Abstract

The paper presents results of the exact three-dimensional analysis of the natural frequencies and mode shapes of a rectangular piezoelectric plate poled along the direction perpendicular to the plate middle plane. The solutions are obtained in non-dimensional form for flexural modes of vibration of a plate simply supported along the plate edges and two types of electrical boundary conditions on the plate faces, namely for the case of short and open circuit. A numerically stable algorithm is described, which allows the calculation of the natural frequencies and mode shapes of the piezoelectric plate. The details of the algorithm have been found to be especially important in the case of equal wavelengths along the two plate edges (e.g. for the lowest flexural mode of a square plate). The natural frequencies of a rectangular plate are given for a rectangular and square plate for the case of short-circuited and open-circuit plate faces, together with the through-thickness distributions of the mechanical and electric fields. Energy balance for piezoelectric continua is used to derive two equivalent formulae which extend the Rayleigh quotient used in free vibration analysis of elastic continua. These expressions are used to verify the consistency of the results and to obtain additional insight into the phenomenon of electromechanical coupling in a vibrating piezoelectric plate.

*Tel.: +48-12-628-3396; fax: +48-12-648-4531.
E-mail address: cupial@mech.pk.edu.pl (P. Cupiał).

0022-460X/$ - see front matter © 2004 Elsevier Ltd. All rights reserved.
doi:10.1016/j.jsv.2004.06.019

Nomenclature

a, b	plate side lengths
A,B,C,D	mode shape constants
c_{ij}	elements of the elastic stiffness matrix
$\mathbf{D}$	electric displacement vector with components (D_x, D_y, D_z)
$\bar{D}_x^{(h)}, \bar{D}_y^{(h)}, \bar{D}_z^{(h)}$	functions of $\bar{z}$ describing through-thickness distribution of non-dimensional components of electric displacement vector
$\mathbf{E}$	electric field vector with components (E_x,E_y,E_z)
e_{ij}	piezoelectric constants
h	plate thickness
k_{ij}	dielectric constants
K	kinetic energy
m, n	number of half-waves along the x- and y-direction
P_{el}	electric power supplied to piezoelectric plate
P_{mech}	mechanical power supplied to piezoelectric plate
$r = a/b$	ratio of plate side lengths
T	matrix transpose
u_x, u_y, u_z	displacements along the co-ordinate axes as functions of (x,y,z,t)
$\bar{U}_x, \bar{U}_y, \bar{U}_z$	amplitudes of non-dimensional displacements as functions of ($\bar{x}, \bar{y}, \bar{z}$)
$\bar{U}_x^{(h)}, \bar{U}_y^{(h)}, \bar{U}_z^{(h)}$	functions of $\bar{z}$ describing through-thickness distribution of non-dimensional displacements
U	internal energy (strain energy + energy of the electric field)
V	volume of the plate
x, y, z	coordinates
$\bar{x}, \bar{y}, \bar{z}$	non-dimensional coordinates
∂V	plate boundary (plate faces and all side planes)
$\varepsilon_x, \varepsilon_y, \varepsilon_z$	strain components
$\gamma_{yz}, \gamma_{xz}, \gamma_{xy}$	engineering shear strains
ϕ	electrostatic potential
$\bar{\Phi}$	amplitude of non-dimensional potential as a function of ($\bar{x}, \bar{y}, \bar{z}$)
$\bar{\Phi}^{(h)}$	function of $\bar{z}$ describing through-thickness distribution of non-dimensional potential
$\xi = a/h$	ratio of plate side length along x-axis to plate thickness
λ_i	eight roots which determine the through-thickness variation of solutions
ρ	mass density
$\sigma_x, \sigma_y, \sigma_z$ $\sigma_{yz}, \sigma_{xz}, \sigma_{xy}$	stress components
$\hat{\sigma}$	free charge per unit area prescribed on the surface of piezoelectric plate
$\bar{\Theta}_x^{(h)}, \bar{\Theta}_y^{(h)}, \bar{\Theta}_z^{(h)}$	functions of $\bar{z}$ describing through-thickness distribution of non-dimensional stresses
$\bar{\Theta}_{yz}^{(h)}, \bar{\Theta}_{xz}^{(h)}, \bar{\Theta}_{xy}^{(h)}$	
$\bar{\omega}_{mn}$	lowest non-dimensional natural frequency of mode (m,n)
$\bar{\omega}_{mn}^{(i)}$	subsequent branches of non-dimensional natural frequencies of mode (m,n)
$(\bar{\cdot})$	non-dimensional quantities
$(\hat{\cdot})$	values prescribed on the boundary
$(\cdot)^{(h)}$	functions of $\bar{z}$ describing through-thickness distributions of mechanical and electric fields

1. Introduction

Piezoelectric materials are used in a number of applications thanks to their ability to convert mechanical energy into electric one and vice versa. Nowadays, the interest in these materials has increased due to their use as sensors and actuators in smart structures. Piezoelectric elements also hold a potential promise of application in microelectromechanical systems (MEMS), miniature mechanical systems integrated with microelectronic elements.

A number of dynamic solutions are available for piezoelectric continua, as discussed e.g. in Refs. [1,2], where solutions are discussed for some wave propagation problems and certain standing wave problems (such as the through-thickness vibration modes).

Some exact results of three-dimensional (3D) static and dynamic analyses of single-layer and multiple-layer rectangular plates are also available in the literature. For a uniform and layered orthotropic plate with no piezoelectric effect, 3D static and natural vibration analysis was done by Srinivas and Rao [3]. Three-dimensional solutions for the static behaviour of a simply supported piezoelectric rectangular plate have been obtained by Bisegna and Maceri [4]. Static solutions for layered piezoelectric simply supported plates are discussed by Heyliger [5], and for more general boundary conditions by Vel and Batra [6].

The number of papers concerning the 3D problem of piezoelectric plate vibration is limited. Exact solutions of the free vibration problem of layered piezoelectric plates are discussed for the case of a plate infinite in one dimension (case of cylindrical bending) in Ref. [7], and for a finite plate in Ref. [8]. In Ref. [8] the natural frequencies and mode shapes of a square uniform plate are calculated as a special case of the multi-layered formulation. However, it is pointed out in this reference that it has been a difficult numerical problem to evaluate the resulting nonlinear eigenvalue problem and the problem is ill-conditioned. In Ref. [9] the natural frequencies of a single-layer rectangular piezoelectric plate have been calculated using a different approach based on the transfer matrix formulation.

Apart from exact solutions, a number of approximate theories of static deformation as well as the vibrations of piezoelectric plates have been proposed. For the static case one can refer to Ref. [10] and the literature therein. For the vibration problems, different approximate plate theories are discussed in Refs. [11–16]. In Ref. [11] asymptotic theory has been used to derive the approximate theory of piezoelectric plates and shells. The theories discussed in Refs. [12–16] use some a priori approximations of the mechanical and electric fields in the through-thickness direction, and the equations of vibration are derived using Hamilton's principle.

The present paper discusses the results of exact 3D analysis of a single-layer piezoelectric rectangular plate. The plate is poled perpendicular to the plate plane and is assumed to be made of a piezoelectric material from the symmetry class 6 mm. A stable numerical algorithm is discussed and natural frequencies and mode shapes are obtained for rectangular and square piezoelectric plates. In order to verify the calculated natural frequencies and mode shapes two expressions are derived in the paper which extend the Rayleigh quotient usually used in the free vibration analysis of elastic bodies. These expressions provide a means of verifying the results and add to the understanding of the electromechanical coupling mechanism in vibrating piezoelectric continua, and to the best of the author's knowledge have not been used before.

2. Three-dimensional equations of piezoelectric plate vibrations

A rectangular plate with the geometry shown in Fig. 1 is considered. The equations of free vibration of a piezoelectric continuum, which are discussed in more detail in Refs. [1,2], consist of the three classical equations of vibration and the electrostatic equation (the Gauss

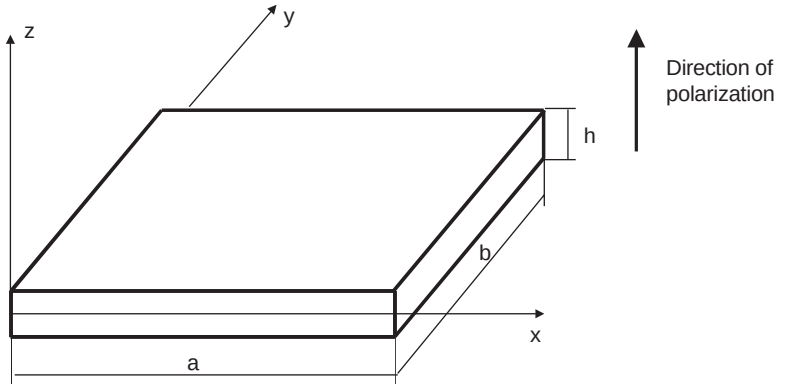

Fig. 1. Rectangular plate poled along the z-axis.

equation of electrostatics):

$$\frac{\partial\sigma_x}{\partial x}+\frac{\partial\sigma_{xy}}{\partial y}+\frac{\partial\sigma_{xz}}{\partial z}=\rho\frac{\partial^2 u_x}{\partial t^2},\quad \frac{\partial\sigma_{xy}}{\partial x}+\frac{\partial\sigma_y}{\partial y}+\frac{\partial\sigma_{yz}}{\partial z}=\rho\frac{\partial^2 u_y}{\partial t^2},$$
$$\frac{\partial\sigma_{xz}}{\partial x}+\frac{\partial\sigma_{yz}}{\partial y}+\frac{\partial\sigma_z}{\partial z}=\rho\frac{\partial^2 u_z}{\partial t^2},\quad \frac{\partial D_x}{\partial x}+\frac{\partial D_y}{\partial y}+\frac{\partial D_z}{\partial z}=0. \tag{1}$$

In Eq. (1), D_x, D_y and D_z are the components of the electric displacement vector. A full list of symbols used throughout the paper is provided in Nomenclature.

The piezoelectric plate is assumed to be made of a ceramic material poled perpendicular to the plate middle plane. The properties of piezoelectric ceramics are discussed in detail in Ref. [17]. An important property of piezoelectric ceramics is their cylindrical symmetry about the poling direction and as a result, as pointed out in Ref. [17], the constitutive equations have the same form as for a crystal with symmetry class 6 mm. For this symmetry class and for a plate poled along the z-axis the physical equations are given by the following equations:

$$\begin{Bmatrix}\sigma_x\\ \sigma_y\\ \sigma_z\\ \sigma_{yz}\\ \sigma_{xz}\\ \sigma_{xy}\end{Bmatrix}=\begin{bmatrix}c_{11}&c_{12}&c_{13}&0&0&0\\ c_{12}&c_{11}&c_{13}&0&0&0\\ c_{13}&c_{13}&c_{33}&0&0&0\\ 0&0&0&c_{44}&0&0\\ 0&0&0&0&c_{44}&0\\ 0&0&0&0&0&c_{66}\end{bmatrix}\begin{Bmatrix}\varepsilon_x\\ \varepsilon_y\\ \varepsilon_z\\ \gamma_{yz}\\ \gamma_{xz}\\ \gamma_{xy}\end{Bmatrix}-\begin{bmatrix}0&0&e_{31}\\ 0&0&e_{31}\\ 0&0&e_{33}\\ 0&e_{15}&0\\ e_{15}&0&0\\ 0&0&0\end{bmatrix}\begin{Bmatrix}E_x\\ E_y\\ E_z\end{Bmatrix}, \tag{2}$$

$$\begin{Bmatrix}D_x\\ D_y\\ D_z\end{Bmatrix}=\begin{bmatrix}0&0&0&0&e_{15}&0\\ 0&0&0&e_{15}&0&0\\ e_{31}&e_{31}&e_{33}&0&0&0\end{bmatrix}\begin{Bmatrix}\varepsilon_x\\ \varepsilon_y\\ \varepsilon_z\\ \gamma_{yz}\\ \gamma_{xz}\\ \gamma_{xy}\end{Bmatrix}+\begin{bmatrix}k_{11}&0&0\\ 0&k_{11}&0\\ 0&0&k_{33}\end{bmatrix}\begin{Bmatrix}E_x\\ E_y\\ E_z\end{Bmatrix}. \tag{3}$$

Here E_x, E_y and E_z are the components of the electric field vector. For the prescribed symmetry class $c_{66} = (c_{11} - c_{12})/2$. It is pointed out that many crystals including quartz have lower symmetry and the present analysis is not valid for them.

The components of the strains and engineering shear measures appearing in physical equations (2) and (3) are given by the classical expressions:

$$\varepsilon_x = \frac{\partial u_x}{\partial x}, \quad \varepsilon_y = \frac{\partial u_y}{\partial y}, \quad \varepsilon_z = \frac{\partial u_z}{\partial z},$$
$$\gamma_{xy} = \frac{\partial u_x}{\partial y} + \frac{\partial u_y}{\partial x}, \quad \gamma_{xz} = \frac{\partial u_x}{\partial z} + \frac{\partial u_z}{\partial x}, \quad \gamma_{yz} = \frac{\partial u_y}{\partial z} + \frac{\partial u_z}{\partial y}. \tag{4}$$

Moreover, using the quasi-static approximation discussed in Ref. [1], which relies on the fact that the mechanical wavelengths are much shorter than the lengths of electromagnetic waves of the same frequency, one can express the electric field vector as a gradient of the electrostatic potential:

$$\mathbf{E} = -\nabla\phi = (-\partial\phi/\partial x, -\partial\phi/\partial y, -\partial\phi/\partial z). \tag{5}$$

Combining Eqs. (1)–(5), a set of four governing equations is obtained in terms of displacements and the electric potential . The analysis will be done in non-dimensional terms and the following non-dimensional quantities are defined:

$$\bar{x} = \frac{x}{a}, \quad \bar{y} = \frac{y}{b}, \quad \bar{z} = \frac{z}{h}, \quad \bar{u}_x = \frac{u_x}{h}, \quad \bar{u}_y = \frac{u_y}{h}, \quad \bar{u}_z = \frac{u_z}{h}, \quad r = \frac{a}{b}, \quad \xi = \frac{a}{h},$$
$$\bar{c}_{11} = \frac{c_{11}}{c_{\text{ref}}}, \quad \bar{c}_{12} = \frac{c_{12}}{c_{\text{ref}}}, \quad \bar{c}_{13} = \frac{c_{13}}{c_{\text{ref}}}, \quad \bar{c}_{33} = \frac{c_{33}}{c_{\text{ref}}}, \quad \bar{c}_{44} = \frac{c_{44}}{c_{\text{ref}}}, \quad \bar{c}_{66} = \frac{c_{66}}{c_{\text{ref}}},$$
$$\bar{e}_{15} = \frac{e_{15}}{e_{\text{ref}}}, \quad \bar{e}_{31} = \frac{e_{31}}{e_{\text{ref}}}, \quad \bar{e}_{33} = \frac{e_{33}}{e_{\text{ref}}}, \quad \bar{k}_{11} = \frac{k_{11}c_{\text{ref}}}{(e_{\text{ref}})^2}, \quad \bar{k}_{33} = \frac{k_{33}c_{\text{ref}}}{(e_{\text{ref}})^2},$$
$$\bar{\phi} = \frac{\phi e_{\text{ref}}}{h c_{\text{ref}}}, \quad \bar{\omega} = \omega a\sqrt{\frac{\rho}{c_{\text{ref}}}}, \quad \bar{t} = \frac{t}{a}\sqrt{\frac{c_{\text{ref}}}{\rho}}. \tag{6}$$

In all numerical calculations the following reference values will be used: $c_{\text{ref}} = c_{11}$ and $e_{\text{ref}} = e_{33}$. When the plate undergoes free vibration:

$$\begin{Bmatrix} \bar{u}_x(\bar{x},\bar{y},\bar{z},\bar{t}) \\ \bar{u}_y(\bar{x},\bar{y},\bar{z},\bar{t}) \\ \bar{u}_z(\bar{x},\bar{y},\bar{z},\bar{t}) \\ \bar{\phi}(\bar{x},\bar{y},\bar{z},\bar{t}) \end{Bmatrix} = \begin{Bmatrix} \bar{U}_x(\bar{x},\bar{y},\bar{z}) \\ \bar{U}_y(\bar{x},\bar{y},\bar{z}) \\ \bar{U}_z(\bar{x},\bar{y},\bar{z}) \\ \bar{\Phi}(\bar{x},\bar{y},\bar{z}) \end{Bmatrix} \sin(\bar{\omega}\bar{t}). \tag{7}$$

With the definitions of amplitudes of displacements and potential (7), the four governing equations of the free vibration problem are written in dimensionless form as follows:

$$\bar{c}_{11}\frac{\partial^2 \bar{U}_x}{\partial \bar{x}^2} + \bar{c}_{66}r^2\frac{\partial^2 \bar{U}_x}{\partial \bar{y}^2} + \bar{c}_{44}\xi^2\frac{\partial^2 \bar{U}_x}{\partial \bar{z}^2} + (\bar{c}_{12} + \bar{c}_{66})r\frac{\partial^2 \bar{U}_y}{\partial \bar{x}\partial \bar{y}} + (\bar{c}_{13} + \bar{c}_{44})\xi\frac{\partial^2 \bar{U}_z}{\partial \bar{x}\partial \bar{z}}$$

$$+(\bar{e}_{15}+\bar{e}_{31})\xi\frac{\partial^2\bar{\Phi}}{\partial\bar{x}\partial\bar{z}}=-\bar{\omega}^2\bar{U}_x, \tag{8}_1$$

$$(\bar{c}_{12}+\bar{c}_{66})r\frac{\partial^2\bar{U}_x}{\partial\bar{x}\partial\bar{y}}+\bar{c}_{66}\frac{\partial^2\bar{U}_y}{\partial\bar{x}^2}+\bar{c}_{11}r^2\frac{\partial^2\bar{U}_y}{\partial\bar{y}^2}+\bar{c}_{44}\xi^2\frac{\partial^2\bar{U}_y}{\partial\bar{z}^2}+(\bar{c}_{13}+\bar{c}_{44})r\xi\frac{\partial^2\bar{U}_z}{\partial\bar{y}\partial\bar{z}}$$
$$+(\bar{e}_{15}+\bar{e}_{31})r\xi\frac{\partial^2\bar{\Phi}}{\partial\bar{y}\partial\bar{z}}=-\bar{\omega}^2\bar{U}_y, \tag{8}_2$$

$$(\bar{c}_{13}+\bar{c}_{44})\xi\frac{\partial^2\bar{U}_x}{\partial\bar{x}\partial\bar{z}}+(\bar{c}_{13}+\bar{c}_{44})r\xi\frac{\partial^2\bar{U}_y}{\partial\bar{y}\partial\bar{z}}+\bar{c}_{44}\frac{\partial^2\bar{U}_z}{\partial\bar{x}^2}+\bar{c}_{44}r^2\frac{\partial^2\bar{U}_z}{\partial\bar{y}^2}+\bar{c}_{33}\xi^2\frac{\partial^2\bar{U}_z}{\partial\bar{z}^2}$$
$$+\bar{e}_{15}\frac{\partial^2\bar{\Phi}}{\partial\bar{x}^2}+\bar{e}_{15}r^2\frac{\partial^2\bar{\Phi}}{\partial\bar{y}^2}+\bar{e}_{33}\xi^2\frac{\partial^2\bar{\Phi}}{\partial\bar{z}^2}=-\bar{\omega}^2\bar{U}_z, \tag{8}_3$$

$$(\bar{e}_{15}+\bar{e}_{31})\xi\frac{\partial^2\bar{U}_x}{\partial\bar{x}\partial\bar{z}}+(\bar{e}_{15}+\bar{e}_{31})r\xi\frac{\partial^2\bar{U}_y}{\partial\bar{y}\partial\bar{z}}+\bar{e}_{15}\frac{\partial^2\bar{U}_z}{\partial\bar{x}^2}+\bar{e}_{15}r^2\frac{\partial^2\bar{U}_z}{\partial\bar{y}^2}+\bar{e}_{33}\xi^2\frac{\partial^2\bar{U}_z}{\partial\bar{z}^2}$$
$$-\bar{k}_{11}\frac{\partial^2\bar{\Phi}}{\partial\bar{x}^2}-\bar{k}_{11}r^2\frac{\partial^2\bar{\Phi}}{\partial\bar{y}^2}-\bar{k}_{33}\xi^2\frac{\partial^2\bar{\Phi}}{\partial\bar{z}^2}=0. \tag{8}_4$$

The set of equations (8) has to be considered together with the respective boundary conditions. For a piezoelectric continuum, the general form of boundary conditions is given as follows (for more details see Refs. [1,2]):

$$u_i=\hat{u}_i \text{ or } \sigma_{ij}n_j=\hat{p}_i;\quad \phi=\hat{\phi} \text{ or } D_in_i=-\hat{\sigma}. \tag{9}$$

In Eq. (9) the index i stands for x, y or z, n_i stands for the components of the outward unit normal to the plate boundary, $\hat{u}_i$, $\hat{p}_i$ and $\hat{\phi}$ are the prescribed displacements, forces and potential, and $\hat{\sigma}$ is the prescribed surface free charge (surface charge not including the polarization charge).

For free vibration analysis all right-hand side terms in conditions (9) are equal to zero and the explicit expressions of the boundary conditions on the plate faces can be written in the following non-dimensional form (which must hold for $\bar{z}=\pm\frac{1}{2}$):

$$\bar{U}_x=0 \text{ or } \bar{c}_{44}(\xi\frac{\partial\bar{U}_x}{\partial\bar{z}}+\frac{\partial\bar{U}_z}{\partial\bar{x}})+\bar{e}_{15}\frac{\partial\bar{\Phi}}{\partial\bar{x}}=0,\quad \bar{U}_y=0 \text{ or } \bar{c}_{44}(\xi\frac{\partial\bar{U}_y}{\partial\bar{z}}+r\frac{\partial\bar{U}_z}{\partial\bar{y}})+\bar{e}_{15}r\frac{\partial\bar{\Phi}}{\partial\bar{y}}=0,$$
$$\bar{U}_z=0 \text{ or } \bar{c}_{13}(\frac{\partial\bar{U}_x}{\partial\bar{x}}+r\frac{\partial\bar{U}_y}{\partial\bar{y}})+\bar{c}_{33}\xi\frac{\partial\bar{U}_z}{\partial\bar{z}}+\bar{e}_{33}\xi\frac{\partial\bar{\Phi}}{\partial\bar{z}}=0,$$
$$\bar{\Phi}=0 \text{ or } \bar{e}_{31}(\frac{\partial\bar{U}_x}{\partial\bar{x}}+r\frac{\partial\bar{U}_y}{\partial\bar{y}})+\bar{e}_{33}\xi\frac{\partial\bar{U}_z}{\partial\bar{z}}-\bar{k}_{33}\xi\frac{\partial\bar{\Phi}}{\partial\bar{z}}=0. \tag{10}$$

3. Solution algorithm

Assuming the boundary conditions of simple support and zero potential along the plate edges, the solution is sought in the form

$$\begin{Bmatrix} \bar{U}_x(\bar{x},\bar{y},\bar{z}) \\ \bar{U}_y(\bar{x},\bar{y},\bar{z}) \\ \bar{U}_z(\bar{x},\bar{y},\bar{z}) \\ \bar{\Phi}(\bar{x},\bar{y},\bar{z}) \end{Bmatrix} = \begin{Bmatrix} \bar{U}_x^{(h)}(\bar{z})\cos(m\pi\bar{x})\sin(n\pi\bar{y}) \\ \bar{U}_y^{(h)}(\bar{z})\sin(m\pi\bar{x})\cos(n\pi\bar{y}) \\ \bar{U}_z^{(h)}(\bar{z})\sin(m\pi\bar{x})\sin(n\pi\bar{y}) \\ \bar{\Phi}^{(h)}(\bar{z})\sin(m\pi\bar{x})\sin(n\pi\bar{y}) \end{Bmatrix}. \tag{11}$$

In Eq. (11), and everywhere in the text, the superscript $^{(h)}$ marks the function which describes the through-thickness distribution of the respective quantity.

Upon introducing solution (11) into the set of equations (8), the problem is reduced to solving a system of ordinary differential equations in $\bar{z}$, with m and n being parameters appearing in the coefficients. One seeks the solution in the z-direction in the following form:

$$\bar{U}_x^{(h)}(\bar{z}) = A\mathrm{e}^{\lambda\bar{z}}, \quad \bar{U}_y^{(h)}(\bar{z}) = B\mathrm{e}^{\lambda\bar{z}}, \quad \bar{U}_z^{(h)}(\bar{z}) = C\mathrm{e}^{\lambda\bar{z}}, \quad \bar{\Phi}^{(h)}(\bar{z}) = D\mathrm{e}^{\lambda\bar{z}}. \tag{12}$$

Upon introducing the solutions (11) and (12) into the governing equations (8), a system of homogenous linear equations in A, B, C and D is obtained. For a non-trivial solution, the determinant must be equal to zero. From this condition eight values of λ are found, for the assumed guess value of $\bar{\omega}$. These eight roots appear as real $\pm$ pairs and complex conjugate pairs. For each of the eight values of λ, three of the four constants A, B, C and D can be expressed as multiples of one of them. In principle, the choice here is arbitrary. However, for the case of equal wave lengths along the plate edges, when $m/a = n/b$ (or $m = r\,n$ in non-dimensional form), most of the 3×3 minors of the 4×4 matrix have been found to be zero from the numerical point of view for two of the roots λ, among them all minors when C or D is taken as the singled-out constant. This kind of problem was encountered for the flexural mode of a square plate with $m = n = 1$ (the results of which are given in Table 4 in the next section) or for mode (2,1) of a rectangular plate of Table 1. In all studied cases, the minors obtained by removing the rows and columns with the constants A and B have been found to be nonzero and the numerical algorithm was stable for the case when $m/a = n/b$. Therefore, we express all coefficients in terms of A, and calculate the remaining coefficients from the last three equations. It is pointed out that if $m/a \neq n/b$ any choice of the singled-out constant was found to give the same results.

The solution in the z-direction is thus obtained in the form

$$\begin{Bmatrix} \bar{U}_x^{(h)}(\bar{z}) \\ \bar{U}_y^{(h)}(\bar{z}) \\ \bar{U}_z^{(h)}(\bar{z}) \\ \bar{\Phi}^{(h)}(\bar{z}) \end{Bmatrix} = \sum_{i=1}^{8} \begin{Bmatrix} 1 \\ \beta_i(\bar{\omega},\lambda_i) \\ \gamma_i(\bar{\omega},\lambda_i) \\ \delta_i(\bar{\omega},\lambda_i) \end{Bmatrix} A_i\mathrm{e}^{\lambda_i\bar{z}}. \tag{13}$$

Expressions (11) and (13) are then introduced into the boundary conditions (10) (any mechanical and electrical boundary condition can be specified on the plate faces). This results in a homogenous system of 8 linear equations in A_i. Again, for non-trivial solution the determinant must be zero. Iteration is done over $\bar{\omega}$ until this condition is met. In the iteration process one first assumes a guess value of $\bar{\omega}$ and changes the value with a rude step until the determinant changes sign. The points where the determinant changes sign define the interval with the frequency sought. This interval is then scanned with a 10 times refined step. By continuing this process it was possible to find the frequency with very high accuracy. It is pointed out that the determinant obtained from the boundary conditions turns out to be either real or purely imaginary, depending on the natural frequency being calculated.

After the natural frequency has been calculated, the through-thickness variation of the mode shapes is found by solving the homogenous system with one arbitrary scaling factor left undetermined. The stress components and the components of the electric displacement vector are then calculated from the known displacements and electric potential using the following formulae:

$$
\begin{aligned}
\bar{\sigma}_x &= \frac{\sigma_x}{c_{\mathrm{ref}}} = \frac{1}{\xi}\left(\bar{c}_{11}\frac{\partial \bar{u}_x}{\partial \bar{x}} + \bar{c}_{12} r \frac{\partial \bar{u}_y}{\partial \bar{y}} + \bar{c}_{13}\xi \frac{\partial \bar{u}_z}{\partial \bar{z}} + \bar{e}_{31}\xi \frac{\partial \bar{\phi}}{\partial \bar{z}}\right),\\
\bar{\sigma}_y &= \frac{\sigma_y}{c_{\mathrm{ref}}} = \frac{1}{\xi}\left(\bar{c}_{12}\frac{\partial \bar{u}_x}{\partial \bar{x}} + \bar{c}_{11} r \frac{\partial \bar{u}_y}{\partial \bar{y}} + \bar{c}_{13}\xi \frac{\partial \bar{u}_z}{\partial \bar{z}} + \bar{e}_{31}\xi \frac{\partial \bar{\phi}}{\partial \bar{z}}\right),\\
\bar{\sigma}_{yz} &= \frac{\sigma_{yz}}{c_{\mathrm{ref}}} = \frac{1}{\xi}\left[\bar{c}_{44}\left(\xi \frac{\partial \bar{u}_y}{\partial \bar{z}} + r\frac{\partial \bar{u}_z}{\partial \bar{y}}\right) + \bar{e}_{15} r \frac{\partial \bar{\phi}}{\partial \bar{y}}\right],\\
\bar{\sigma}_{xz} &= \frac{\sigma_{xz}}{c_{\mathrm{ref}}} = \frac{1}{\xi}\left[\bar{c}_{44}\left(\xi \frac{\partial \bar{u}_x}{\partial \bar{z}} + \frac{\partial \bar{u}_z}{\partial \bar{x}}\right) + \bar{e}_{15}\frac{\partial \bar{\phi}}{\partial \bar{x}}\right],\\
\bar{\sigma}_{xy} &= \frac{\sigma_{xy}}{c_{\mathrm{ref}}} = \frac{\bar{c}_{66}}{\xi}\left(r\frac{\partial \bar{u}_x}{\partial \bar{y}} + \frac{\partial \bar{u}_y}{\partial \bar{x}}\right),\\
\bar{\sigma}_z &= \frac{\sigma_z}{c_{\mathrm{ref}}} = \frac{1}{\xi}\left[\bar{c}_{13}\left(\frac{\partial \bar{u}_x}{\partial \bar{x}} + r\frac{\partial \bar{u}_y}{\partial \bar{y}}\right) + \bar{c}_{33}\xi \frac{\partial \bar{u}_z}{\partial \bar{z}} + \bar{e}_{33}\xi \frac{\partial \bar{\phi}}{\partial \bar{z}}\right],
\end{aligned}
$$

$$
\begin{aligned}
\bar{D}_x &= \frac{D_x}{e_{\mathrm{ref}}} = \frac{1}{\xi}\left[\bar{e}_{15}\left(\xi \frac{\partial \bar{u}_x}{\partial \bar{z}} + \frac{\partial \bar{u}_z}{\partial \bar{x}}\right) - \bar{k}_{11}\frac{\partial \bar{\phi}}{\partial \bar{x}}\right],\\
\bar{D}_y &= \frac{D_y}{e_{\mathrm{ref}}} = \frac{1}{\xi}\left[\bar{e}_{15}\left(\xi \frac{\partial \bar{u}_y}{\partial \bar{z}} + r\frac{\partial \bar{u}_z}{\partial \bar{y}}\right) - \bar{k}_{11} r \frac{\partial \bar{\phi}}{\partial \bar{y}}\right],\\
\bar{D}_z &= \frac{D_z}{e_{\mathrm{ref}}} = \frac{1}{\xi}\left[\bar{e}_{31}\left(\frac{\partial \bar{u}_x}{\partial \bar{x}} + r\frac{\partial \bar{u}_y}{\partial \bar{y}}\right) + \bar{e}_{33}\xi \frac{\partial \bar{u}_z}{\partial \bar{z}} - \bar{k}_{33}\xi \frac{\partial \bar{\phi}}{\partial \bar{z}}\right].
\end{aligned}
\tag{14}
$$

As in the case of displacements and the electrostatic potential, the stress components and the electric vector components vary harmonically along the x- and y-axis in the

following manner:

$$\begin{Bmatrix} \bar{\sigma}_x(\bar{x},\bar{y},\bar{z},\bar{t}) \\ \bar{\sigma}_y(\bar{x},\bar{y},\bar{z},\bar{t}) \\ \bar{\sigma}_z(\bar{x},\bar{y},\bar{z},\bar{t}) \\ \bar{\sigma}_{yz}(\bar{x},\bar{y},\bar{z},\bar{t}) \\ \bar{\sigma}_{xz}(\bar{x},\bar{y},\bar{z},\bar{t}) \\ \bar{\sigma}_{xy}(\bar{x},\bar{y},\bar{z},\bar{t}) \end{Bmatrix} = \begin{Bmatrix} \bar{\Theta}_x^{(h)}(\bar{z})\sin(m\pi\bar{x})\sin(n\pi\bar{y}) \\ \bar{\Theta}_y^{(h)}(\bar{z})\sin(m\pi\bar{x})\sin(n\pi\bar{y}) \\ \bar{\Theta}_z^{(h)}(\bar{z})\sin(m\pi\bar{x})\sin(n\pi\bar{y}) \\ \bar{\Theta}_{yz}^{(h)}(\bar{z})\sin(m\pi\bar{x})\cos(n\pi\bar{y}) \\ \bar{\Theta}_{xz}^{(h)}(\bar{z})\cos(m\pi\bar{x})\sin(n\pi\bar{y}) \\ \bar{\Theta}_{xy}^{(h)}(\bar{z})\cos(m\pi\bar{x})\cos(n\pi\bar{y}) \end{Bmatrix} \sin(\bar{\omega}\,\bar{t}), \tag{15}$$

$$\begin{Bmatrix} \bar{D}_x(\bar{x},\bar{y},\bar{z},\bar{t}) \\ \bar{D}_y(\bar{x},\bar{y},\bar{z},\bar{t}) \\ \bar{D}_z(\bar{x},\bar{y},\bar{z},\bar{t}) \end{Bmatrix} = \begin{Bmatrix} \bar{D}_x^{(h)}(\bar{z})\cos(m\pi\bar{x})\sin(n\pi\bar{y}) \\ \bar{D}_y^{(h)}(\bar{z})\sin(m\pi\bar{x})\cos(n\pi\bar{y}) \\ \bar{D}_z^{(h)}(\bar{z})\sin(m\pi\bar{x})\sin(n\pi\bar{y}) \end{Bmatrix} \sin(\bar{\omega}\bar{t}). \tag{16}$$

4. Numerical results

In this section numerical results will be discussed for rectangular and square plates free from mechanical tractions on the faces and for two different electrical boundary conditions, namely the case of short-circuited (shorted) plate faces ($\phi = 0$ on both faces) and open-circuit faces ($D_z = 0$ on both faces). In non-dimensional form, the mechanical boundary conditions are given explicitly by the second relations in the first three equations of Eq. (10) and the electrical boundary condition is given by the first or second expression of the fourth equation (10). The following material constants for the ceramic PZT4 taken from Ref. [18] are used in the calculations:

$$\begin{aligned} &c_{11} = 13.2\times10^{10}(\mathrm{N/m^2}), \quad c_{12} = 7.1\times10^{10}(\mathrm{N/m^2}), \quad c_{13} = 7.3\times10^{10}(\mathrm{N/m^2}),\\ &c_{33} = 11.5\times10^{10}(\mathrm{N/m^2}), \quad c_{44} = 2.6\times10^{10}(\mathrm{N/m^2}), \quad c_{66} = 3.0\times10^{10}(\mathrm{N/m^2}),\\ &e_{15} = 10.5(\mathrm{C/m^2}), \quad e_{31} = -4.1(\mathrm{C/m^2}), \quad e_{33} = 14.1(\mathrm{C/m^2}),\\ &k_{11} = 7.124\times10^{-9}(\mathrm{F/m}), \quad k_{33} = 5.841\times10^{-9}(\mathrm{F/m}), \quad \rho = 7.5\times10^{3}(\mathrm{kg/m^3}). \end{aligned} \tag{17}$$

Similar values of the material constants for the PZT4 ceramic are also given in Ref. [19].

Table 1 shows the non-dimensional circular frequencies $\bar{\omega}_{mn}$, for $m,n = 1,2,3$, for a thin rectangular plate with $r = a/b = 2$ and $\xi = a/h = 100$, for the case of short-circuited plate faces. For each pair (m,n) the frequency corresponding to the lowest frequency branch is shown. Similar results for the case of open-circuit faces are included in Table 2. It is pointed out, that for the modes in question (lowest frequency branch for a given m and n) one of the two electrical boundary conditions used has very little effect on the frequencies shown in Tables 1 and 2. This conclusion agrees with the results for the corresponding modes obtained from 3D analysis in Ref. [8] and from a two-dimensional theory in Ref. [16]. Table 3 includes the natural frequencies

Table 1
Lowest non-dimensional circular frequencies of a rectangular plate with $r = a/b = 2$ and $\xi = a/h = 100$

m	n		
	1	2	3
1	$\bar{\omega}_{11} = 0.1287$	$\bar{\omega}_{12} = 0.4368$	$\bar{\omega}_{13} = 0.9476$
2	$\bar{\omega}_{21} = 0.2056$	$\bar{\omega}_{22} = 0.5132$	$\bar{\omega}_{23} = 1.023$
3	$\bar{\omega}_{31} = 0.3338$	$\bar{\omega}_{32} = 0.6405$	$\bar{\omega}_{33} = 1.149$

The case of short-circuited plate faces ($\phi = 0$ on the faces).

Table 2
Lowest non-dimensional circular frequencies of a rectangular plate with $r = a/b = 2$ and $\xi = a/h = 100$

m	n		
	1	2	3
1	$\bar{\omega}_{11} = 0.1287$	$\bar{\omega}_{12} = 0.4370$	$\bar{\omega}_{13} = 0.9482$
2	$\bar{\omega}_{21} = 0.2056$	$\bar{\omega}_{22} = 0.5134$	$\bar{\omega}_{23} = 1.024$
3	$\bar{\omega}_{31} = 0.3339$	$\bar{\omega}_{32} = 0.6408$	$\bar{\omega}_{33} = 1.150$

The case of open-circuit plate faces ($D_z = 0$ on the faces).

Table 3
Lowest non-dimensional circular frequencies of a rectangular plate with $r = a/b = 2$ and $\xi = a/h = 100$

m	n		
	1	2	3
1	$\bar{\omega}_{11} = 0.1144$	$\bar{\omega}_{12} = 0.3887$	$\bar{\omega}_{13} = 0.8430$
2	$\bar{\omega}_{21} = 0.1828$	$\bar{\omega}_{22} = 0.4564$	$\bar{\omega}_{23} = 0.9102$
3	$\bar{\omega}_{31} = 0.2969$	$\bar{\omega}_{32} = 0.5696$	$\bar{\omega}_{33} = 1.022$

The case of elastic plate without electromechanical coupling.

of a plate with the same geometry as in Tables 1 and 2 but with the electromechanical coupling not accounted for. These results were obtained by solving the purely mechanical vibration problem with the constitutive equations (2) in which all piezoelectric constants were assumed to be equal to zero. Comparing results in Tables 1 and 2 with those of Table 3 it is observed that the natural frequencies with piezoelectric coupling are higher than those with no coupling. This fact will be further explained in Section 5.2, using energy concepts.

The plots of the through-thickness variation of the non-dimensional displacements and stress components are shown in Fig. 2. The plots are given for the mode (1,1) of a rectangular plate with the geometry and natural frequencies as in Tables 1 and 2. Almost the same mechanical fields are obtained for the case of short-circuited and open-circuit plate faces. The corresponding

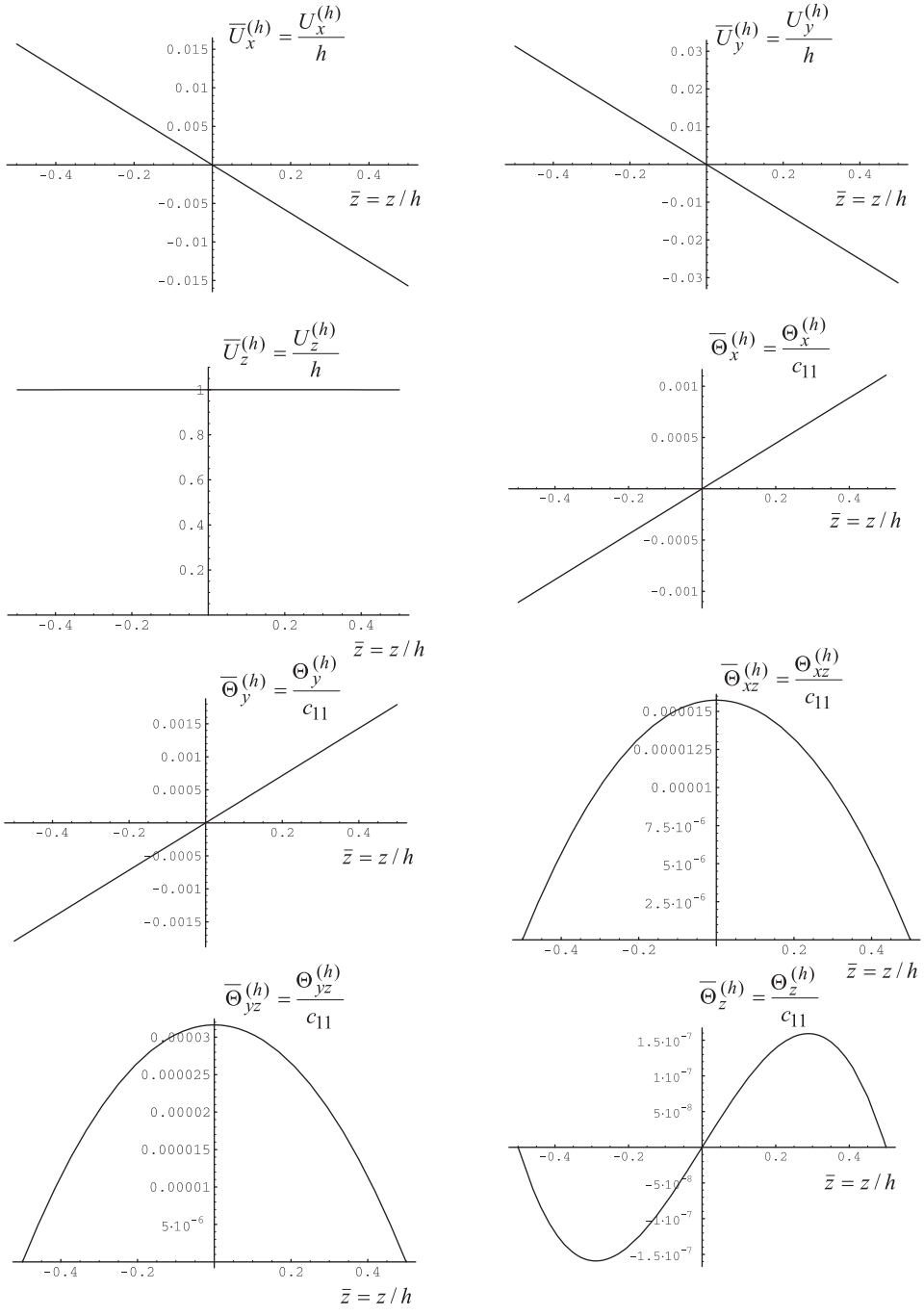

Fig. 2. Through-thickness variation of non-dimensional displacements and stress components for the lowest mode of a rectangular plate with $r = a/b = 2$ and $\xi = a/h = 100$ (almost the same shapes of mechanical fields were obtained for the case of short-circuited plate faces ($\phi = 0$) and open-circuit faces ($D_z = 0$)).

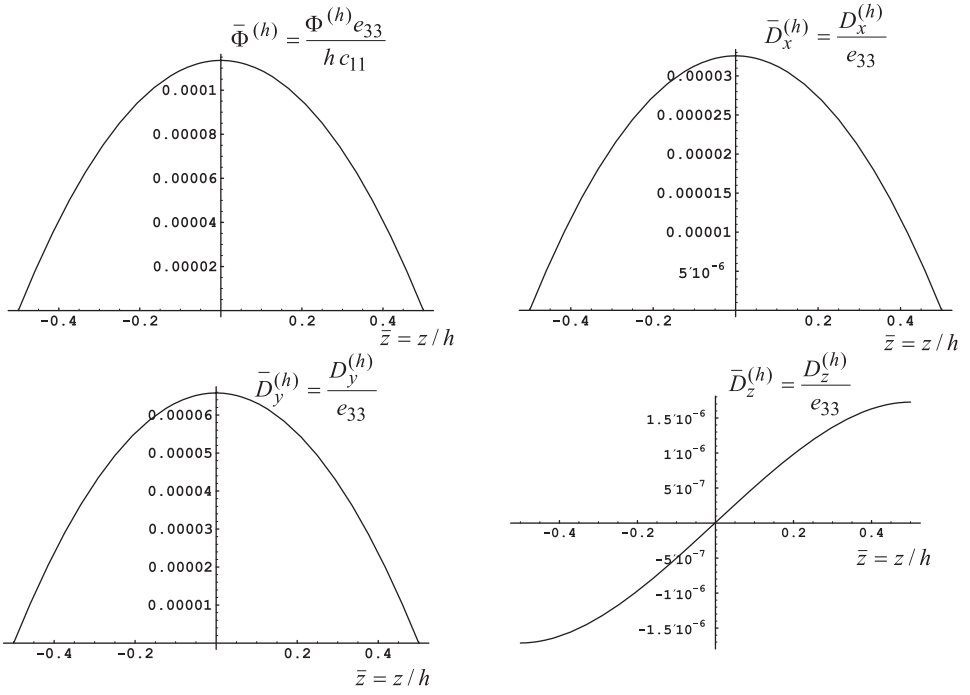

Fig. 3. Through-thickness variation of the electric fields for the lowest mode of a rectangular plate with $r = a/b = 2$ and $\xi = a/h = 100$, for the case of short-circuited plate faces ($\phi = 0$ on both faces).

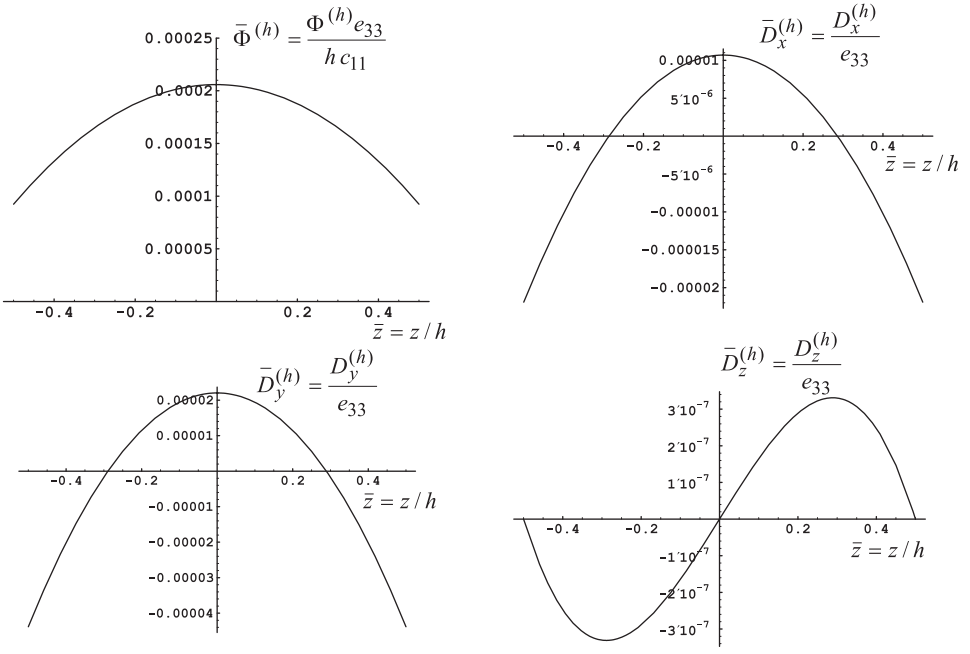

Fig. 4. Through-thickness variation of the electric fields for the lowest mode of a rectangular plate with $r = a/b = 2$ and $\xi = a/h = 100$, for the case of open-circuit plate faces ($D_z = 0$ on both faces).

through-thickness distribution of the electric fields is shown in Figs. 3 and 4, respectively, for the case of short- and open circuit.

The calculated natural frequencies and the values of the mechanical and electric fields were verified by comparing with finite element results obtained using the coupled-field capability of the finite element code ANSYS. The comparison of the natural frequencies is included in Ref. [20], for the rectangular plate of Tables 1 and 2. Good agreement was obtained for both frequencies and the calculated fields.

Table 4 shows the natural frequencies calculated for a thin square plate, for the case of shorted faces. Again, the natural frequencies of a plate with open faces differ very little from those included in Table 4. The natural frequencies of a thick plate with $\xi = a/h = 10$ and shorted faces are shown in Tables 5 and 6, respectively, for a rectangular and a square plate. Even though for

Table 4
Lowest non-dimensional circular frequencies of a square plate with $r = a/b = 1$ and $\xi = a/h = 100$

m	n		
	1	2	3
1	$\bar{\omega}_{11} = 0.0514$	$\bar{\omega}_{12} = 0.1287$	$\bar{\omega}_{13} = 0.2572$
2	$\bar{\omega}_{21} = 0.1287$	$\bar{\omega}_{22} = 0.2056$	$\bar{\omega}_{23} = 0.3338$
3	$\bar{\omega}_{31} = 0.2572$	$\bar{\omega}_{32} = 0.3338$	$\bar{\omega}_{33} = 0.4616$

The case of short-circuited plate faces ($\phi = 0$ on the faces).

Table 5
Lowest non-dimensional circular frequencies of a rectangular plate with $r = a/b = 2$ and $\xi = a/h = 10$

m	n		
	1	2	3
1	$\bar{\omega}_{11} = 1.1863$	$\bar{\omega}_{12} = 3.4983$	$\bar{\omega}_{13} = 6.4858$
2	$\bar{\omega}_{21} = 1.8200$	$\bar{\omega}_{22} = 3.9972$	$\bar{\omega}_{23} = 6.8750$
3	$\bar{\omega}_{31} = 2.7866$	$\bar{\omega}_{32} = 4.7824$	$\bar{\omega}_{33} = 7.5002$

The case of short-circuited plate faces ($\phi = 0$ on the faces).

Table 6
Lowest non-dimensional circular frequencies of a square plate with $r = a/b = 1$ and $\xi = a/h = 10$

m	n		
	1	2	3
1	$\bar{\omega}_{11} = 0.4969$	$\bar{\omega}_{12} = 1.1863$	$\bar{\omega}_{13} = 2.2211$
2	$\bar{\omega}_{21} = 1.1863$	$\bar{\omega}_{22} = 1.8200$	$\bar{\omega}_{23} = 2.7866$
3	$\bar{\omega}_{31} = 2.2211$	$\bar{\omega}_{32} = 2.7866$	$\bar{\omega}_{33} = 3.6639$

The case of short-circuited plate faces ($\phi = 0$ on the faces).

Table 7
Consecutive frequency branches for mode (1,1) of a rectangular plate with $r = a/b = 2$ and $\xi = a/h = 10$

Short-circuited faces	$\bar{\omega}_{11}^{(1)} = 1.1863$	$\bar{\omega}_{11}^{(2)} = 5.6006$	$\bar{\omega}_{11}^{(3)} = 14.345$	$\bar{\omega}_{11}^{(4)} = 15.170$
Open-circuit faces	$\bar{\omega}_{11}^{(1)} = 1.1948$	$\bar{\omega}_{11}^{(2)} = 6.2847$	$\bar{\omega}_{11}^{(3)} = 14.345$	$\bar{\omega}_{11}^{(4)} = 17.902$

Table 8
Consecutive frequency branches for mode (1,1) of a square plate with $r = a/b = 1$ and $\xi = a/h = 10$

Short-circuited faces	$\bar{\omega}_{11}^{(1)} = 0.4969$	$\bar{\omega}_{11}^{(2)} = 3.5568$	$\bar{\omega}_{11}^{(3)} = 14.107$	$\bar{\omega}_{11}^{(4)} = 14.457$
Open-circuit faces	$\bar{\omega}_{11}^{(1)} = 0.4985$	$\bar{\omega}_{11}^{(2)} = 3.9963$	$\bar{\omega}_{11}^{(3)} = 14.107$	$\bar{\omega}_{11}^{(4)} = 17.183$

the thicker plate the difference between the frequencies of the closed- and open-circuit case is bigger than for thin plates, this difference is still small and the corresponding values of the frequencies for the open case are not given explicitly (for the mode (1,1) the effect of the electrical boundary conditions can be read from Tables 7 and 8).

All the results discussed so far concerned the lowest natural frequencies calculated for a given (m,n). However, higher frequency branches exist for each (m,n) with mode shape distributions which can differ from those shown in Figs. 2–4. The numerical algorithm of Section 3 proved equally efficient in calculating these branches. Tables 7 and 8 show the lowest four branches of the mode (1,1) of a shorted and open case, for a rectangular and square plate with $\xi = a/h = 10$. The frequencies of the lowest branch $\bar{\omega}_{11}^{(1)}$ coincide with the values shown in the earlier tables. By comparing the values in Tables 7 and 8 it is seen that the electrical boundary conditions used can have an important effect on the frequencies of some of the higher frequency modes.

5. Verification of the calculated natural frequencies and mode shapes

5.1. Verification of some identities valid on the plate faces

In order to verify the consistency of the results, it is interesting to explain the following properties of the plots of the through-thickness distributions of the electric potential and the components of the electric displacement vector shown in Figs. 3 and 4. In the case of short-circuited plate faces ($\phi = 0$ on both faces) the calculated x- and y- components of the electric displacement vector are equal to zero on the plate faces, as can be seen from plots in Fig. 3. For the case of open-circuit faces both the potential and the x- and y-components of the electric displacement vector are non-zero, as is seen from Fig. 4. A simple relation between the potential and the in-plane electric displacement components can be derived, to check for the accuracy of the results calculated numerically. Since in both cases studied the plate faces are

free from surface tractions, $\sigma_{xz} = \sigma_{yz} = 0$ on the faces. Then, from the physical equations (2) it follows that $\gamma_{xz} = (e_{15}/c_{44})E_x = -(e_{15}/c_{44})\partial\phi/\partial x$ and $\gamma_{yz} = (e_{15}/c_{44})E_y = -(e_{15}/c_{44})\partial\phi/\partial y$. Introducing these relations into the second set of constitutive equations, and using the definitions of non-dimensional quantities (6) one arrives at the following relations, which must hold on the face layers free from mechanical tractions:

$$\bar{D}_x = -\bar{k}_{11}\left(1 + \frac{\bar{e}_{15}^2}{\bar{c}_{44}\bar{k}_{11}}\right)\frac{1}{\xi}\frac{\partial\bar{\phi}}{\partial\bar{x}} \quad \text{and} \quad \bar{D}_y = -\bar{k}_{11}\left(1 + \frac{\bar{e}_{15}^2}{\bar{c}_{44}\bar{k}_{11}}\right)\frac{r}{\xi}\frac{\partial\bar{\phi}}{\partial\bar{y}}. \tag{18}$$

In the case of shorted electrodes $\bar{\phi} = 0$ everywhere on both faces and thus $\bar{D}_x = \bar{D}_y = 0$ on the plate faces, in agreement with the plots shown in Fig. 3. As a check of the consistency of numerical results shown in Fig. 4, Eqs. (18) were also verified to hold to high accuracy for the case of open-circuit faces.

5.2. Verification of results using energy concepts

In order to further verify the consistency of the calculated natural frequencies and mode shapes as well as obtain additional insight into the mechanism of electromechanical coupling in a vibrating piezoelectric plate, formulae will be derived which generalize to piezoelectricity the Rayleigh quotient used in the free vibration of elastic continua. Two such expressions are derived below using the governing equations $(8)_1$–$(8)_4$ of the free vibration problem. A different derivation, directly from the energy balance for a piezoelectric continuum is given in Appendix A.

To obtain the first expression of the Rayleigh quotient, one starts with the equations of free vibrations $(8)_1$–$(8)_3$, which can be written in the following equivalent form:

$$\begin{aligned}&\frac{\partial}{\partial\bar{x}}\left(\bar{c}_{11}\frac{\partial\bar{U}_x}{\partial\bar{x}} + \bar{c}_{12}r\frac{\partial\bar{U}_y}{\partial\bar{y}} + \bar{c}_{13}\xi\frac{\partial\bar{U}_z}{\partial\bar{z}} + \bar{e}_{31}\xi\frac{\partial\bar{\Phi}}{\partial\bar{z}}\right) + r\frac{\partial}{\partial\bar{y}}\left[\bar{c}_{66}\left(r\frac{\partial\bar{U}_x}{\partial\bar{y}} + \frac{\partial\bar{U}_y}{\partial\bar{x}}\right)\right]\\ &\quad + \xi\frac{\partial}{\partial\bar{z}}\left[\bar{c}_{44}\left(\xi\frac{\partial\bar{U}_x}{\partial\bar{z}} + \frac{\partial\bar{U}_z}{\partial\bar{x}}\right) + \bar{e}_{15}\frac{\partial\bar{\Phi}}{\partial\bar{x}}\right] = -\bar{\omega}_{mn}^2\bar{U}_x,\end{aligned} \tag{19}_1$$

$$\begin{aligned}&\frac{\partial}{\partial\bar{x}}\left[\bar{c}_{66}\left(r\frac{\partial\bar{U}_x}{\partial\bar{y}} + \frac{\partial\bar{U}_y}{\partial\bar{x}}\right)\right] + r\frac{\partial}{\partial\bar{y}}\left(\bar{c}_{12}\frac{\partial\bar{U}_x}{\partial\bar{x}} + \bar{c}_{11}r\frac{\partial\bar{U}_y}{\partial\bar{y}} + \bar{c}_{13}\xi\frac{\partial\bar{U}_z}{\partial\bar{z}} + \bar{e}_{31}\xi\frac{\partial\bar{\Phi}}{\partial\bar{z}}\right)\\ &\quad + \xi\frac{\partial}{\partial\bar{z}}\left[\bar{c}_{44}\left(\xi\frac{\partial\bar{U}_y}{\partial\bar{z}} + r\frac{\partial\bar{U}_z}{\partial\bar{y}}\right) + \bar{e}_{15}r\frac{\partial\bar{\Phi}}{\partial\bar{y}}\right] = -\bar{\omega}_{mn}^2\bar{U}_y,\end{aligned} \tag{19}_2$$

$$\begin{aligned}&\frac{\partial}{\partial\bar{x}}\left[\bar{c}_{44}\left(\xi\frac{\partial\bar{U}_x}{\partial\bar{z}} + \frac{\partial\bar{U}_z}{\partial\bar{x}}\right) + \bar{e}_{15}\frac{\partial\bar{\Phi}}{\partial\bar{x}}\right] + r\frac{\partial}{\partial\bar{y}}\left[\bar{c}_{44}\left(\xi\frac{\partial\bar{U}_y}{\partial\bar{z}} + r\frac{\partial\bar{U}_z}{\partial\bar{y}}\right) + \bar{e}_{15}r\frac{\partial\bar{\Phi}}{\partial\bar{y}}\right]\\ &\quad + \xi\frac{\partial}{\partial\bar{z}}\left[\bar{c}_{13}\left(\frac{\partial\bar{U}_x}{\partial\bar{x}} + r\frac{\partial\bar{U}_y}{\partial\bar{y}}\right) + \bar{c}_{33}\xi\frac{\partial\bar{U}_z}{\partial\bar{z}} + \bar{e}_{33}\xi\frac{\partial\bar{\Phi}}{\partial\bar{z}}\right] = -\bar{\omega}_{mn}^2\bar{U}_z.\end{aligned} \tag{19}_3$$

Here, the functions $\bar{U}_x, \bar{U}_y, \bar{U}_z, \bar{\Phi}$ are the mode shapes corresponding to the frequency $\bar{\omega}_{mn}$. One multiplies Eqs. $(19)_1$–$(19)_3$ respectively by $\bar{U}_x, \bar{U}_y, \bar{U}_z$ and integrates over the plate volume. Integrating by parts over $\bar{x}, \bar{y}$ and $\bar{z}$ and using the boundary conditions (10) (specified on the plate faces) and the boundary conditions of simple support and zero potential on the plate sides (which are satisfied by the assumed shapes (11)) one can show that the boundary terms vanish, and the following expression for the Rayleigh quotient is obtained:

$$\bar{\omega}_{mn}^2 = \frac{\text{Num}}{\text{Denom}}, \tag{20}$$

$$\begin{aligned}\text{Num} = \int_0^1 \int_0^1 \int_{-1/2}^{1/2} \Bigg[& \bar{c}_{11}\left(\frac{\partial \bar{U}_x}{\partial \bar{x}}\right)^2 + \bar{c}_{11} r^2 \left(\frac{\partial \bar{U}_y}{\partial \bar{y}}\right)^2 + \bar{c}_{33}\xi^2 \left(\frac{\partial \bar{U}_z}{\partial \bar{z}}\right)^2 + 2\bar{c}_{12} r \frac{\partial \bar{U}_x}{\partial \bar{x}} \frac{\partial \bar{U}_y}{\partial \bar{y}} \\ & + 2\bar{c}_{13}\xi \frac{\partial \bar{U}_x}{\partial \bar{x}} \frac{\partial \bar{U}_z}{\partial \bar{z}} + 2\bar{c}_{13} r\xi \frac{\partial \bar{U}_y}{\partial \bar{y}} \frac{\partial \bar{U}_z}{\partial \bar{z}} + \bar{c}_{44}\left(\xi \frac{\partial \bar{U}_x}{\partial \bar{z}} + \frac{\partial \bar{U}_z}{\partial \bar{x}}\right)^2 + \bar{c}_{44}\left(\xi \frac{\partial \bar{U}_y}{\partial \bar{z}} + r \frac{\partial \bar{U}_z}{\partial \bar{y}}\right)^2 \\ & + \bar{c}_{66}\left(r \frac{\partial \bar{U}_x}{\partial \bar{y}} + \frac{\partial \bar{U}_y}{\partial \bar{x}}\right)^2 + \bar{e}_{15} \frac{\partial \bar{\Phi}}{\partial \bar{x}} \left(\xi \frac{\partial \bar{U}_x}{\partial \bar{z}} + \frac{\partial \bar{U}_z}{\partial \bar{x}}\right) + \bar{e}_{15} r \frac{\partial \bar{\Phi}}{\partial \bar{y}} \left(\xi \frac{\partial \bar{U}_y}{\partial \bar{z}} + r \frac{\partial \bar{U}_z}{\partial \bar{y}}\right) \\ & + \xi \frac{\partial \bar{\Phi}}{\partial \bar{z}} \left(\bar{e}_{31} \frac{\partial \bar{U}_x}{\partial \bar{x}} + \bar{e}_{31} r \frac{\partial \bar{U}_y}{\partial \bar{y}} + \bar{e}_{33}\xi \frac{\partial \bar{U}_z}{\partial \bar{z}}\right) \Bigg] \mathrm{d}\bar{x}\, \mathrm{d}\bar{y}\, \mathrm{d}\bar{z}, \end{aligned} \tag{21}$$

$$\text{Denom} = \int_0^1 \int_0^1 \int_{-1/2}^{1/2} (\bar{U}_x^2 + \bar{U}_y^2 + \bar{U}_z^2)\, \mathrm{d}\bar{x}\, \mathrm{d}\bar{y}\, \mathrm{d}\bar{z}. \tag{22}$$

An alternative expression of the Rayleigh quotient can be obtained using the electrostatic equation (8_4), which can be written in the following form:

$$\begin{aligned} & \frac{\partial}{\partial \bar{x}} \left[\bar{e}_{15}\left(\xi \frac{\partial \bar{U}_x}{\partial \bar{z}} + \frac{\partial \bar{U}_z}{\partial \bar{x}}\right) - \bar{k}_{11} \frac{\partial \bar{\Phi}}{\partial \bar{x}}\right] + r \frac{\partial}{\partial \bar{y}} \left[\bar{e}_{15}\left(\xi \frac{\partial \bar{U}_y}{\partial \bar{z}} + r \frac{\partial \bar{U}_z}{\partial \bar{y}}\right) - \bar{k}_{11} r \frac{\partial \bar{\Phi}}{\partial \bar{y}}\right] \\ & \quad + \xi \frac{\partial}{\partial \bar{z}} \left[\bar{e}_{31}\left(\frac{\partial \bar{U}_x}{\partial \bar{x}} + r \frac{\partial \bar{U}_y}{\partial \bar{y}}\right) + \bar{e}_{33}\xi \frac{\partial \bar{U}_z}{\partial \bar{z}} - \bar{k}_{33}\xi \frac{\partial \bar{\Phi}}{\partial \bar{z}}\right] = 0. \end{aligned} \tag{23}$$

One multiplies Eq. (21) by $\bar{\Phi}$ and integrates over the volume of the plate. Performing integration by parts and using the fact that the boundary terms can be shown to vanish, the following identity is obtained:

$$\begin{aligned} \int_0^1 \int_0^1 \int_{-1/2}^{1/2} \Bigg\{ & \left[\bar{e}_{15}\left(\xi \frac{\partial \bar{U}_x}{\partial \bar{z}} + \frac{\partial \bar{U}_z}{\partial \bar{x}}\right) - \bar{k}_{11} \frac{\partial \bar{\Phi}}{\partial \bar{x}}\right] \frac{\partial \bar{\Phi}}{\partial \bar{x}} + \left[\bar{e}_{15}\left(\xi \frac{\partial \bar{U}_y}{\partial \bar{z}} + r \frac{\partial \bar{U}_z}{\partial \bar{y}}\right) - \bar{k}_{11} r \frac{\partial \bar{\Phi}}{\partial \bar{y}}\right] r \frac{\partial \bar{\Phi}}{\partial \bar{y}} \\ & + \left[\bar{e}_{31}\left(\frac{\partial \bar{U}_x}{\partial \bar{x}} + r \frac{\partial \bar{U}_y}{\partial \bar{y}}\right) + \bar{e}_{33}\xi \frac{\partial \bar{U}_z}{\partial \bar{z}} - \bar{k}_{33}\xi \frac{\partial \bar{\Phi}}{\partial \bar{z}}\right] \xi \frac{\partial \bar{\Phi}}{\partial \bar{z}} \Bigg\} \mathrm{d}\bar{x}\, \mathrm{d}\bar{y}\, \mathrm{d}\bar{z} = 0. \end{aligned} \tag{24}$$

Using relation (24) in Eq. (22) the following equivalent expression for the numerator of the Rayleigh quotient is obtained:

$$\begin{aligned}\text{Num} = \int_0^1 \int_0^1 \int_{-1/2}^{1/2} \Bigg[& \bar{c}_{11}\left(\frac{\partial \bar{U}_x}{\partial \bar{x}}\right)^2 + \bar{c}_{11} r^2 \left(\frac{\partial \bar{U}_y}{\partial \bar{y}}\right)^2 + \bar{c}_{33}\xi^2 \left(\frac{\partial \bar{U}_z}{\partial \bar{z}}\right)^2 + 2\bar{c}_{12} r \frac{\partial \bar{U}_x}{\partial \bar{x}} \frac{\partial \bar{U}_y}{\partial \bar{y}} \\ & + 2\bar{c}_{13}\xi \frac{\partial \bar{U}_x}{\partial \bar{x}} \frac{\partial \bar{U}_z}{\partial \bar{z}} + 2\bar{c}_{13} r\xi \frac{\partial \bar{U}_y}{\partial \bar{y}} \frac{\partial \bar{U}_z}{\partial \bar{z}} + \bar{c}_{44}\left(\xi \frac{\partial \bar{U}_x}{\partial \bar{z}} + \frac{\partial \bar{U}_z}{\partial \bar{x}}\right)^2 + \bar{c}_{44}\left(\xi \frac{\partial \bar{U}_y}{\partial \bar{z}} + r \frac{\partial \bar{U}_z}{\partial \bar{y}}\right)^2 \\ & + \bar{c}_{66}\left(r \frac{\partial \bar{U}_x}{\partial \bar{y}} + \frac{\partial \bar{U}_y}{\partial \bar{x}}\right)^2 + \bar{k}_{11}\left(\frac{\partial \bar{\Phi}}{\partial \bar{x}}\right)^2 + \bar{k}_{11} r^2 \left(\frac{\partial \bar{\Phi}}{\partial \bar{y}}\right)^2 + \bar{k}_{33}\xi^2 \left(\frac{\partial \bar{\Phi}}{\partial \bar{z}}\right)^2 \Bigg] \mathrm{d}\bar{x}\,\mathrm{d}\bar{y}\,\mathrm{d}\bar{z}. \end{aligned} \tag{25}$$

This can be used in quotient (20) with the denominator defined as previously (Eq. (22)).

Both expressions of the Rayleigh quotient have been used to check for the consistency of the calculated natural frequencies and mode shapes. The calculated mode shapes were introduced into any of the two expressions of the quotient and thus the natural frequency has been calculated in a different way. The same frequencies have been found using any of the two quotients, which were in perfect agreement with the value found as a solution of the eigenvalue problem.

The derived expressions of the Rayleigh quotients can be used to provide additional insight into the electromechanical coupling phenomenon in the vibrating piezoelectric plate. To illustrate this let us take the case of a rectangular plate with $r = a/b = 2$ and $\xi = a/h = 100$. For this plate the natural frequencies calculated for two different electrical boundary conditions were found to be very close for the lowest frequency branch, as shown in Tables 1 and 2. However, these values are higher than the corresponding values without a piezoelectric coupling (as seen by comparing with Table 3). To investigate electromechanical coupling, one can split numerator (25) into the mechanical part (including only displacements) and the electrical part (with electrostatic potential only). For the plate geometry of Tables 1 and 2, for both shorted and open electrical boundary conditions on the plate faces, these terms are very close, and for the mode (1,1) the mechanical part accounts for 84% of the overall numerator value whereas the electrical part for 16%. As a result, the electric field is not negligible and results in natural frequencies higher than for a plate without the electromechanical coupling.

Furthermore, using the plots in Figs. 2–4 it is possible to justify why the natural frequencies in Tables 1 and 2 depend little on one of the two electrical boundary conditions used. In fact, the electrical contribution to the numerator (25) is given by

$$\int_0^1 \int_0^1 \int_{-1/2}^{1/2} \left[\bar{k}_{11}\left(\frac{\partial \bar{\Phi}}{\partial \bar{x}}\right)^2 + \bar{k}_{11} r^2 \left(\frac{\partial \bar{\Phi}}{\partial \bar{y}}\right)^2 + \bar{k}_{33}\xi^2 \left(\frac{\partial \bar{\Phi}}{\partial \bar{z}}\right)^2 \right] \mathrm{d}\bar{x}\,\mathrm{d}\bar{y}\,\mathrm{d}\bar{z}. \tag{26}$$

The first two terms are small compared to the third one, especially for thin plates for which ξ is high. It is also seen from Figs. 3 and 4 that for the two electrical boundary conditions used the potential varies almost quadratically in the thickness direction. One can verify from the plots that the quadratic term coefficient is almost the same in both cases. Since the linear term is zero (both plots have zero derivative at $\bar{z} = 0$) the two potential distributions are very close, with the exception of a constant term. As a result the last derivative in Eq. (26) is very much the same for the two cases and the contribution of the electrical part is almost the same. Since the mechanical

shapes are very similar for the two cases, the natural frequencies of the modes in question are not sensitive to electrical boundary conditions, especially for thin plates.

It is also pointed out that the mechanical fields calculated from the coupled problem are not identical to those calculated from the uncoupled elastic problem. The natural frequency calculated from the mechanical part of quotient (20) (using the displacements calculated from the coupled problem) for mode (1,1) of the rectangular plate with $r = a/b = 2$ and $\xi = a/h = 100$ was found to be equal 0.1178. The square root of the corresponding quotient in the absence of electromechanical coupling (which is equal to the natural frequency), can be read from Table 3 and is equal to 0.1144.

6. Conclusions

The approach discussed in the paper allows the exact 3D analysis of the natural frequencies of simply supported rectangular plates with arbitrary boundary conditions specified on the plate faces, as well as introduces energy concepts which add greatly to the understanding of the obtained results. The algorithm used is numerically stable, but the details of the algorithm were found to be important in the case when $m/a = n/b$, as explained in Section 3. Numerical results were obtained for rectangular and square plates with faces free from mechanical tractions and for two different electrical boundary conditions applied on the plate faces, namely for the case of shorted faces ($\phi = 0$) or the case of open faces ($D_z = 0$). For both electrical boundary conditions studied, a strong electromechanical coupling exists. This is reflected e.g. by a high value of electric potential generated during vibration (for the case of shorted faces shown in Fig. 3 and the plate thickness $h = 0.001$ (m) the maximum potential during vibration with the first mode shape with amplitude equal to one tenth of the plate thickness is found to be about 100 V). In spite of this coupling, the natural frequencies of the lowest flexural modes are almost the same for the two kinds of boundary conditions used. This is unlike in the case of through-thickness vibration modes (which have been discussed e.g. in Ref. [1]) where one can show that the type of electrical boundary conditions has an important effect on the natural frequencies, and unlike for some higher frequency branches calculated in the present paper. Energy concepts have been used to derive two expressions which extend the Rayleigh quotient applied in the free vibration analysis of elastic structures. These expressions have been found valuable in the verification of the consistency of the calculated natural frequencies and the mode shapes and in the study of the effect of the electromechanical coupling in the vibrating piezoelectric plate.

Appendix A

In this appendix, an outline is given of an alternative derivation of Eqs. (20)–(22) and (25), which extend the Rayleigh quotient to the free vibration of piezoelectric continua.

The balance of energy of a piezoelectric continuum can be written in the following form (more details can be found in Ref. [1,2]):

$$\frac{\mathrm{d}}{\mathrm{d}t}(K + U) = P_{\mathrm{mech}} + P_{\mathrm{el}}. \tag{A.1}$$

In Eq. (A.1), K stands for the kinetic energy of the plate, U is the overall internal energy (which consists of the strain energy and the energy of the electric field), P_{mech} and P_{el} are respectively the mechanical and electric power supplied to the piezoelectric continuum. These quantities are defined as follows:

$$K = \frac{1}{2}\int_V \rho\left[\left(\frac{\partial u_x}{\partial t}\right)^2 + \left(\frac{\partial u_y}{\partial t}\right)^2 + \left(\frac{\partial u_z}{\partial t}\right)^2\right] \mathrm{d}V, \tag{A.2}$$

$$U = \frac{1}{2}\int_V \left[\begin{Bmatrix} \varepsilon_x \\ \varepsilon_y \\ \varepsilon_z \\ \gamma_{yz} \\ \gamma_{xz} \\ \gamma_{xy} \end{Bmatrix}^{\mathrm{T}} \begin{bmatrix} c_{11} & c_{12} & c_{13} & 0 & 0 & 0 \\ c_{12} & c_{11} & c_{13} & 0 & 0 & 0 \\ c_{13} & c_{13} & c_{33} & 0 & 0 & 0 \\ 0 & 0 & 0 & c_{44} & 0 & 0 \\ 0 & 0 & 0 & 0 & c_{44} & 0 \\ 0 & 0 & 0 & 0 & 0 & c_{66} \end{bmatrix} \begin{Bmatrix} \varepsilon_x \\ \varepsilon_y \\ \varepsilon_z \\ \gamma_{yz} \\ \gamma_{xz} \\ \gamma_{xy} \end{Bmatrix} + \begin{Bmatrix} \dfrac{\partial\phi}{\partial x} \\ \dfrac{\partial\phi}{\partial y} \\ \dfrac{\partial\phi}{\partial z} \end{Bmatrix}^{\mathrm{T}} \begin{bmatrix} k_{11} & 0 & 0 \\ 0 & k_{11} & 0 \\ 0 & 0 & k_{33} \end{bmatrix} \begin{Bmatrix} \dfrac{\partial\phi}{\partial x} \\ \dfrac{\partial\phi}{\partial y} \\ \dfrac{\partial\phi}{\partial z} \end{Bmatrix}\right] \mathrm{d}V, \tag{A.3}$$

$$P_{\mathrm{mech}} = \int_V \left(F_x\frac{\partial u_x}{\partial t} + F_y\frac{\partial u_y}{\partial t} + F_z\frac{\partial u_z}{\partial t}\right)\mathrm{d}V + \int_{\partial V}\left(\hat{p}_x\frac{\partial u_x}{\partial t} + \hat{p}_y\frac{\partial u_y}{\partial t} + \hat{p}_z\frac{\partial u_z}{\partial t}\right)\mathrm{d}(\partial V), \tag{A.4}$$

$$P_{\mathrm{el}} = -\int_V \left(\frac{\partial\phi}{\partial x}\frac{\partial D_x}{\partial t} + \frac{\partial\phi}{\partial y}\frac{\partial D_y}{\partial t} + \frac{\partial\phi}{\partial z}\frac{\partial D_z}{\partial t}\right)\mathrm{d}V = -\int_{\partial V}\phi\left(n_x\frac{\partial D_x}{\partial t} + n_y\frac{\partial D_y}{\partial t} + n_z\frac{\partial D_z}{\partial t}\right)\mathrm{d}(\partial V). \tag{A.5}$$

Here F_x, F_y, F_z are components of the mechanical forces per unit volume, $\hat{p}_x$, $\hat{p}_y$, $\hat{p}_z$ are components of the prescribed surface tractions, V is the volume of the plate, ∂V is the plate boundary (consisting of the plate faces and sides), n_x, n_y, n_z are the components of the unit outward normal to the plate boundary.

For free vibration, the volume forces and the surface tractions on the plate faces vanish. Moreover, it can be verified using the assumed fields (11) that there is no mechanical power supplied to the plate through the plate sides. Similarly, using second of formulae (A.5) one can show that for free vibration no electric power is supplied to the system. As a result, conservation of energy holds:

$$\frac{\mathrm{d}}{\mathrm{d}t}(K + U) = 0. \tag{A.6}$$

For free vibration,

$$\begin{Bmatrix} u_x(x,y,z,t) \\ u_y(x,y,z,t) \\ u_z(x,y,z,t) \\ \phi(x,y,z,t) \end{Bmatrix} = \begin{Bmatrix} U_x(x,y,z) \\ U_y(x,y,z) \\ U_z(x,y,z) \\ \Phi(x,y,z) \end{Bmatrix} \sin(\omega_{mn}t). \tag{A.7}$$

Introducing relations (A.7) into the balance of energy (A.6) one can obtain the following equation for the natural frequency:

$$\omega_{mn}^2 = \frac{\text{Num}}{\text{Denom}}, \tag{A.8}$$

where

$$\begin{aligned}\text{Num} = \int_0^a \int_0^b \int_{-h/2}^{h/2} \Bigg[& c_{11}\left(\frac{\partial U_x}{\partial x}\right)^2 + c_{11}\left(\frac{\partial U_y}{\partial y}\right)^2 + c_{33}\left(\frac{\partial U_z}{\partial z}\right)^2 + 2c_{12}\frac{\partial U_x}{\partial x}\frac{\partial U_y}{\partial y} \\ & + 2c_{13}\frac{\partial U_x}{\partial x}\frac{\partial U_z}{\partial z} + 2c_{13}\frac{\partial U_y}{\partial y}\frac{\partial U_z}{\partial z} + c_{44}\left(\frac{\partial U_x}{\partial z} + \frac{\partial U_z}{\partial x}\right)^2 + c_{44}\left(\frac{\partial U_y}{\partial z} + \frac{\partial U_z}{\partial y}\right)^2 \\ & + c_{66}\left(\frac{\partial U_x}{\partial y} + \frac{\partial U_y}{\partial x}\right)^2 + k_{11}\left(\frac{\partial \Phi}{\partial x}\right)^2 + k_{11}\left(\frac{\partial \Phi}{\partial y}\right)^2 + k_{33}\left(\frac{\partial \Phi}{\partial z}\right)^2 \Bigg] \mathrm{d}x\,\mathrm{d}y\,\mathrm{d}z \end{aligned} \tag{A.9}$$

and

$$\text{Denom} = \int_0^a \int_0^b \int_{-h/2}^{h/2} \rho(U_x^2 + U_y^2 + U_z^2)\,\mathrm{d}x\,\mathrm{d}y\,\mathrm{d}z. \tag{A.10}$$

Using non-dimensional quantities, this is identical to formulae (20), (25) and (22), derived in Section 5.2 directly from the governing equations of the problem.

An alternative formula for the numerator of the Rayleigh quotient can be obtained by replacing the surface integral by the volume integral according to formula (A.5), and using the energy balance in the form:

$$\frac{\mathrm{d}}{\mathrm{d}t}(K + U) = -\int_V \left(\frac{\partial \phi}{\partial x}\frac{\partial D_x}{\partial t} + \frac{\partial \phi}{\partial y}\frac{\partial D_y}{\partial t} + \frac{\partial \phi}{\partial z}\frac{\partial D_z}{\partial t}\right) \mathrm{d}V. \tag{A.11}$$

As a result, the equivalent expression for the numerator of the Rayleigh quotient reads as follows:

$$\begin{aligned}\text{Num} = \int_0^a \int_0^b \int_{-h/2}^{h/2} \Bigg[& c_{11}\left(\frac{\partial U_x}{\partial x}\right)^2 + c_{11}\left(\frac{\partial U_y}{\partial y}\right)^2 + c_{33}\left(\frac{\partial U_z}{\partial z}\right)^2 + 2c_{12}\frac{\partial U_x}{\partial x}\frac{\partial U_y}{\partial y} \\ & + 2c_{13}\frac{\partial U_x}{\partial x}\frac{\partial U_z}{\partial z} + 2c_{13}\frac{\partial U_y}{\partial y}\frac{\partial U_z}{\partial z} + c_{44}\left(\frac{\partial U_x}{\partial z} + \frac{\partial U_z}{\partial x}\right)^2 + c_{44}\left(\frac{\partial U_y}{\partial z} + \frac{\partial U_z}{\partial y}\right)^2 \\ & + c_{66}\left(\frac{\partial U_x}{\partial y} + \frac{\partial U_y}{\partial x}\right)^2 + e_{15}\frac{\partial \Phi}{\partial x}\left(\frac{\partial U_x}{\partial z} + \frac{\partial U_z}{\partial x}\right) + e_{15}\frac{\partial \Phi}{\partial y}\left(\frac{\partial U_y}{\partial z} + \frac{\partial U_z}{\partial y}\right) \\ & + \frac{\partial \Phi}{\partial z}\left(e_{31}\frac{\partial U_x}{\partial x} + e_{31}\frac{\partial U_y}{\partial y} + e_{33}\frac{\partial U_z}{\partial z}\right) \Bigg] \mathrm{d}x\,\mathrm{d}y\,\mathrm{d}z. \end{aligned} \tag{A.12}$$

In non-dimensional form expression (A.12) is identical to formula (21) of Section 5.2.

References

[1] H.F. Tiersten, *Linear Piezoelectric Plate Vibrations*, Plenum Press, New York, 1969.

[2] W. Nowacki, *Electromagnetic Effects in Deformable Solids*, (in Polish), Polska Akademia Nauk (Polish Academy of Sciences), Warsaw, 1983.

[3] S. Srinivas, A.K. Rao, Bending, vibration and buckling of simply supported thick orthotropic rectangular plates and laminates, *International Journal of Solids and Structures* 6 (1970) 1463–1481.

[4] P. Bisegna, F. Maceri, An exact three-dimensional solution for simply supported rectangular piezoelectric plates, *Journal of Applied Mechanics* 63 (1996) 628–638.

[5] P. Heyliger, Exact solutions for simply supported laminated piezoelectric plates, *Journal of Applied Mechanics* 64 (1997) 299–306.

[6] S.S. Vel, R.C. Batra, Three-dimensional analytical solution for hybrid multilayered piezoelectric plates, *Journal of Applied Mechanics* 67 (2000) 558–567.

[7] P. Heyliger, S. Brooks, Free vibration of piezoelectric laminates in cylindrical bending, *International Journal of Solids and Structures* 32 (1995) 2945–2960.

[8] P. Heyliger, D.A. Saravanos, Exact free-vibration analysis of laminated plates with embedded piezoelectric layers, *Journal of the Acoustical Society of America* 98 (1995) 1547–1557.

[9] W.-Q. Chen, R.-Q. Xu, H.-J. Ding, On free vibration of a piezoelectric composite rectangular plate, *Journal of Sound and Vibration* 218 (1998) 741–748.

[10] P. Bisegna, G. Caruso, Evaluation of higher-order theories of piezoelectric plates in bending and in stretching, *International Journal of Solids and Structures* 38 (2001) 8805–8830.

[11] N.N. Rogacheva, *The Theory of Piezoelectric Shells and Plates*, CRC Press, Boca Raton, 1994.

[12] J.A. Mitchell, J.N. Reddy, A refined hybrid plate theory for composite laminates with piezoelectric laminae, *International Journal of Solids and Structures* 32 (1995) 2345–2367.

[13] H.S. Tzou, Active piezoelectric shell continua, in: H.S. Tzou, G.L. Anderson (Eds.), *Intelligent Structures and their Applications*, Kluwer Academic Publishers, Amsterdam, 1992.

[14] A. Fernandes, J. Pouget, Accurate modelling of piezoelectric plates: single-layered plate, *Archive of Applied Mechanics* 71 (2001) 509–524.

[15] M. Krommer, H. Irschik, A Reissner-Mindlin type plate theory including the direct piezoelectric and the pyroelectric effect, *Acta Mechanica* 141 (2000) 51–69.

[16] A. Benjeddou, J.-F. Deü, A two-dimensional closed-form solution for the free-vibration analysis of piezoelectric sandwich plates, *International Journal of Solids and Structures* 39 (2002) 1463–1486.

[17] B. Jaffe, W.R. Cook, H. Jaffe, *Piezoelectric Ceramics*, Academic Press, London and New York, 1971.

[18] *ANSYS Verification Guide*, 2nd Ed., SAS IP, Inc.

[19] D. Royer, E. Dieulesaint, *Elastic Waves in Solids*, Springer, Berlin, 2000.

[20] P. Cupiał, Exact three-dimensional natural vibration analysis of a piezoelectric rectangular plate, in: *Proceedings of the VIII International Conference on Recent Advances in Structural Dynamics,* Paper No. 43, Southampton, 2003.